Pergamon

Polyhedron Vol. 14, No. 23–24, pp. 3473–3480, 1995

0277-5387/95 $9.50 + 0.00

0277-5387(95)00205-7

NEW MANGANESE PYROPHOSPHATES: THE SYNTHESES, CRYSTALLOGRAPHIC CHARACTERIZATIONS AND MAGNETIC PROPERTIES OF $BaMnP_2O_7$ AND $CaMnP_2O_7$

RICHARD D. ADAMS* and RALPH LAYLAND

Department of Chemistry and Biochemistry, University of South Carolina, Columbia, SC 29208, U.S.A.

and

CHRISTOPHE PAYEN*

Institut des Matériaux de Nantes, 2 rue de la Houssinière, 44072 Nantes Cedex 03, France

(*Received* 20 *February* 1995; *accepted* 5 *May* 1995)

Abstract—The new compound $BaMnP_2O_7$ was obtained in two crystallographic modifications, (monoclinic-**1**) and (triclinic-**2**), by heating mixtures of $BaCO_3$, P_2O_5 and MnO_2 to 1100°C and to 1000°C for 72 h, respectively. $CaMnP_2O_7$ (**3**) was obtained by heating a mixture of $CaCO_3$, P_2O_5 and MnO_2 to 1050°C for 48 h. Both crystallographic forms of $BaMnP_2O_7$ and $CaMnP_2O_7$ (**3**) were investigated by single-crystal X-ray diffraction analysis. The high-temperature monoclinic form of $BaMnP_2O_7$ could not be obtained free of the low-temperature triclinic form in the bulk form. In monoclinic-**1** the manganese ions exist in a distorted MnO_6 octahedron surrounded by five closely and one remotely positioned oxygen atoms. In triclinic-**2** and -**3** forms the manganese ions are associated in pairs by the formation of Mn_2O_{10} units that share one edge of two adjacent octahedra. The magnetic properties of the triclinic-**2** and -**3** forms were also investigated. The effective magnetic moments, μ_{eff}, are 5.7 B.M. and 5.8 B.M./Mn atom for triclinic-**2** and -**3**, respectively, and are consistent with a high-spin Mn^{2+} ion in an octahedral environment with five unpaired electrons. The temperature-dependent magnetic measurements of **2** and **3** have revealed a combination of short-range antiferromagnetic coupling, J, between the two Mn ions within the Mn_2O_{10} units and a longer range weaker antiferromagnetic coupling, J', between the neighbouring Mn_2O_{10} units, $|J'/J| = 0.18$ and 0.074 for **2** and **3**, respectively.

A variety of mixed-metal pyrophosphates of the type $MM'(P_2O_7)$, $M = M^+ =$ alkali, $M' = M^{3+} =$ transition metal,[1] $M = M^{2+} =$ alkaline earth, $M' = M^{2+} =$ transition metal[2] and $M_2(P_2O_7)$, M = transition metal,[3] have been prepared and characterized. Recently, mixed transition metal pyrophosphates of the type $MM'(P_2O_7)$, $M \neq M'$, have attracted attention because of their ability to form non-stoichiometric solid solutions that exhibit interesting magnetic properties.[4]

We have now prepared and investigated the magnetic properties of two new manganese pyrophosphate compounds, $BaMn(P_2O_7)$ and $CaMn(P_2O_7)$. $BaMn(P_2O_7)$ has been found to exist in two polymorphs: monoclinic-**1** and triclinic-**2**, but only triclinic-**2** could be obtained in a pure form. The manganese ions of triclinic-$BaMn(P_2O_7)$ and $CaMn(P_2O_7)$ exist in pairs in the form of edge-shared Mn_2O_{10} bioctahedral units. Their temperature-dependent magnetic properties show the

*Authors to whom correspondence should be addressed.

effects of both significant short range antiferromagnetic coupling within the bioctahedra and a weaker long range antiferromagnetic coupling between the bioctahedral units.

EXPERIMENTAL

$BaCO_3$ (98%), P_2O_5 (99.99%), MnO_2 (98%) and $CaCO_3$ (99.9%) were purchased from Aldrich and used without further purification. The compounds were heated in a Thermolyne Model F21125 tube furnace. X-ray powder diffraction measurements were performed on a Rigaku powder diffractometer using Cu-K_α radiation (λ = 1.5418 Å).

Synthesis of $BaMnP_2O_7$-*monoclinic* (**1**)

A mixture of $BaCO_3$ (0.987 g, 5.00 mmol), MnO_2 (0.435 g, 5.00 mmol) and P_2O_5 (0.710 g, 5.00 mmol) was ground thoroughly in a mortar, and then transferred to a ceramic crucible. The crucible was then placed in the tube furnace and heated in air to 1100°C for 72 h. At the end of the heating period, the furnace was cooled slowly (approximately 5°C min^{-1}) to room temperature. At this temperature the sample was removed from the oven. A yellow crystal was cleaved from the bulk sample and analysed by single-crystal diffraction. It was found to belong to the monoclinic crystal system.

Synthesis of $BaMnP_2O_7$-*triclinic* (**2**)

A mixture of $BaCO_3$ (0.987 g, 5.00 mmol), MnO_2 (0.436 g, 5.01 mmol) and P_2O_5 (0.710 g, 5.00 mmol) was ground thoroughly in a mortar, and then transferred to a ceramic crucible. The crucible was then placed in the oven (Thermolyne Model F21125) and heated in air to 1000°C for 72 h. After the heating period, the oven was cooled slowly (approx. 5°C min^{-1}) to room temperature. At this temperature the sample was removed from the oven. A yellow crystal was cleaved from the bulk sample and analysed by single-crystal diffractometry. It was found to belong to the triclinic crystal system. An X-ray powder diffraction analysis indicated the bulk sample to be the pure triclinic form.

Synthesis of $CaMnP_2O_7$-*triclinic* (**3**)

A mixture of $CaCO_3$ (0.600 g, 6.00 mmol), MnO_2 (0.5227 g, 6.01 mmol) and P_2O_5 (0.852 g, 6.00 mmol) was ground thoroughly in a mortar, and then transferred to a ceramic crucible. The crucible was then placed in the oven (Thermolyne Model F21125) and heated in air to 1050°C for 48 h. After the heating period, the oven was cooled slowly (approx. 5°C min^{-1}) to room temperature. At this temperature the sample was removed from the oven. A yellow crystal was cleaved from the bulk sample and analysed by single-crystal diffraction. It was found to belong to the triclinic crystal system. An X-ray powder diffraction analysis showed the bulk sample to be pure $CaMnP_2O_7$.

Magnetic measurements

Magnetic measurements were performed on a Quantum Design SQUID magnetometer. The measurements were corrected for diamagnetism and the effects of the sample holder. The sample was first cooled in the absence of an applied field. The susceptibility was then measured upon warming in a static field of 5 kOe.

$BaMnP_2O_7$-*triclinic* (**2**). Magnetic measurements were performed using $BaMnP_2O_7$ (93.41 mg) in the triclinic phase in a powder form.

$CaMnP_2O_7$ (**3**). Magnetic measurements were performed on a sample consisting of $CaMnP_2O_7$ (38.90 mg) in a powder form.

Crystallographic analyses

All crystals used for intensity measurements were mounted in thin-walled glass capillaries. Unit cells were determined from 15 randomly selected reflections obtained by using the AFC6 automatic search, centre, index and least-squares routines. Crystal data, data collection parameters and results of the analyses are listed in Table 1. All data processing was performed on a Digital Equipment Corporation VAXstation 3520 computer using the TEXSAN structure solving program library obtained from the Molecular Structure Corporation, The Woodlands, TX, U.S.A. Lorentz–polarization (Lp) and absorption corrections were applied to the data in each analysis. Neutral atom scattering factors were calculated by the standard procedures.[5a] Anomalous dispersion corrections were applied to all non-hydrogen atoms.[5b] Full-matrix least-squares refinements minimized the function: $\Sigma_{hkl} w(|F_o| - |F_c|)^2$, where $w = 1/\sigma(F)^2$, $\sigma(F) = \sigma(F_o^2)/2F_o$ and $\sigma(F_o^2) = [\sigma(I_{raw})^2 + (0.02I_{net})^2]^{1/2}/Lp$. In each analysis the intensities of three standard reflections were measured every 150 reflections. These showed no significant deviations during the data collection process.

For **1** the space group $P2_1/n$ was established from the patterns of systematic absences observed during the collection of the intensity data. The structure was solved by a combination of direct methods

Table 1. Crystal data for compounds **1–3**

	1	**2**	**3**
Formula	$BaMnP_2O_7$	$BaMnP_2O_7$	$CaMnP_2O_7$
Formula weight	366.21	366.21	268.96
Crystal system	Monoclinic	Triclinic	Triclinic
Lattice parameters			
a (Å)	12.825(2)	5.473(1)	6.6203(8)
b (Å)	8.633(2)	7.593(1)	6.6271(8)
c (Å)	5.5537(6)	7.166(1)	6.5809(6)
α (°)	90	102.10(1)	96.520(9)
β (°)	90.08(1)	86.03(1)	92.648(9)
γ (°)	90	89.29(1)	65.943(8)
V (Å^3)	614.9(1)	290.35	261.94(5)
Space group	$P2_1/n$ (No. 14)	$P\bar{1}$ (No. 2)	$P\bar{1}$ (No. 2)
Z value	2	2	2
ρ_{calc} (g cm^{-3})	1.98	4.19	3.41
μ (Mo-K_α) (cm^{-1})	44.60	94.45	40.85
Temperature (°C)	20	20	20
$2\theta_{max}$ (°)	46.0	50.0	52.0
No. obs. ($I > 3\sigma$)	669	913	927
Goodness of fit	1.16	1.78	2.56
Residuals: R; R_w	0.024; 0.024	0.025; 0.030	0.024; 0.031
Absorption correction	Empirical	Empirical	Empirical
Largest peak in final difference map	0.76	0.90	0.40

$R = \Sigma_{hkl}(||F_{obs}| - |F_{calc}||/\Sigma_{hkl}|F_{obs}|$; $R_w = [\Sigma_{hkl}w(|F_{obs}| - |F_{calc}|^2)/\Sigma_{hkl}wF_{obs}^2]^{1/2}$, $w = 1/\sigma^2(F_{obs})$; GOF $= [\Sigma_{hkl}(|F_{obs}| - |F_{calc}|/\sigma(F_{obs})]/(n_{data} - n_{vari})$.

(MITHRIL) and difference Fourier syntheses. All atoms were refined with anisotropic thermal parameters.

For **2** and **3** the space group $P\bar{1}$ was assumed and confirmed by the successful solution and refinement of the structures. The structures were solved by a combination of direct methods (MITHRIL) and difference Fourier syntheses. All atoms were refined with anisotropic thermal parameters in both analyses.

RESULTS AND DISCUSSION

$BaMnP_2O_7$ was obtained in two crystallographic modifications. A high-temperature monoclinic form **1** was formed at 1100°C and a lower temperature triclinic form **2** was formed at 1000°C. Unfortunately, the high-temperature form was always contaminated with small amounts of the low-temperature form. As a result, magnetic measurements on **1** were not performed.

Description of the structure of $BaMnP_2O_7$*-monoclinic* (**1**)

A projection of the solid-state structure of monoclinic-**1** is shown in Fig. 1. A list of selected bond distances and angles is given in Table 2. The coordination about the manganese ions can be described alternatively as square-pyramidal MnO_5 or distorted-octahedral MnO_6 with five short and one long Mn···O contact. Square pyramidal polyhedra are shown in Fig. 1. All oxygen atoms surrounding the manganese ions are, of course, derived from the pyrophosphate groups. The five short Mn—O contacts range from 2.059(6) to 2.249(5) Å, with the average equal to 2.151 Å. The sixth oxygen atom lies above the centre of the square base at a distance of 2.833(6) Å. Two previously reported compounds, α-$Ca_2(P_2O_7)$[6] and $CaCu(P_2O_7)$,[2b] are isomorphous to monoclinic-**1**, but the structure is much more closely related to that of $CaCu(P_2O_7)$ in which the Cu ion has a square-pyramidal coordination with a sixth long contact in a pseudo-octahedral site. The MnO_5 square pyramids are joined via O—P—O links from the P_2O_7 groups. The average P—O bonding distance is 1.537 Å. The P—O bonds involving the bridging P—O—P atom, O(7), are the longest, as expected, P(1)—O(7) = 1.590(6) and P(2)—O(7) = 1.622(6) Å. Each diphosphate unit has one oxygen atom which participates in the coordination to the Ba ion only. Each barium ion has nine proximate oxygen atoms lying in the range 2.672(6)–3.240(5) Å.

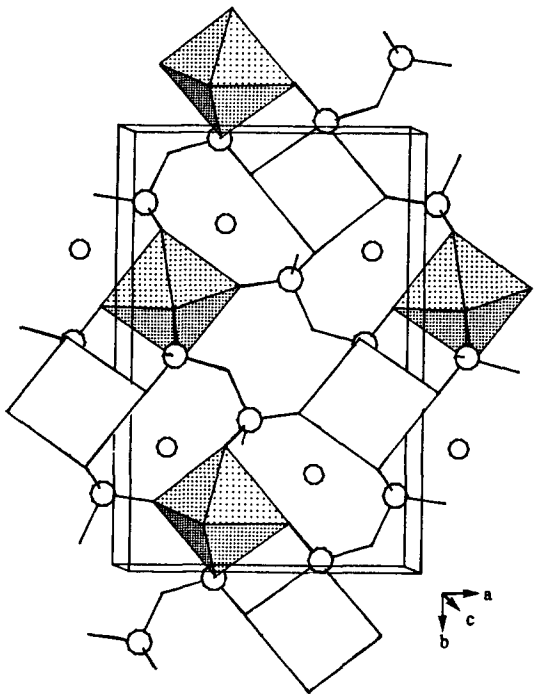

Fig. 1. A plot of the solid-state structure of $BaMnP_2O_7$, monoclinic-**1** projected on to the *ab* lattice plane. The polyhedra show the coordination about the Mn^{2+} ions. The base of the square pyramid is not stippled. Bonds between the phosphorus atoms (large circles) and oxygen atoms are shown, but the oxygen atoms are not drawn. The contacts to the barium atoms (small circles) are not drawn.

Description of the structure of $BaMnP_2O_7$, *triclinic-*(**2**)

A projection of the solid-state structure of triclinic-**2** is shown in Fig. 2. A list of selected bond distances and angles is given in Table 3. The coordination about the manganese ions in triclinic-**2** also can be described either as square-pyramidal MnO_5 or pseudo-octahedral MnO_6 with five short and one long Mn···O contact. Pseudo-octahedral polyhedra are shown in Fig. 2. The five short Mn—O contacts range from 2.095(5) to 2.257(5) Å with the average equal to 2.159 Å. The sixth oxygen atom lies at a bond distance of 2.955(8) Å. Three previously reported compounds, $BaCu(P_2O_7)$,[2d] $BaCo(P_2O_7)$[2e] and $BaNi(P_2O_7)$[2e] are isomorphous to triclinic-**2**. Unlike monoclinic-**1**, the manganese ions are arranged in pairs through the formation of Mn_2O_{10} dinuclear groups in which two octahedra share a common edge. Thus, there is a Mn···Mn contact of 3.413(3) Å within each Mn_2O_{10} group. The Mn_2O_{10} groups are joined via O—P—O links to six nearest-neighbour Mn_2O_{10} groups. The average P—O bonding distance is 1.537 Å. The P—O bonds involving the bridging P—O—P atom, O(4), are the longest, as expected, P(1)—O(4) = 1.611(5) and P(2)—O(4) = 1.608(5) Å. As in monoclinic-**1**, each barium ion has nine proximate oxygen atoms lying in the range 2.749(5)–2.989(5) Å.

Table 2. Selected interatomic distances (Å) and angles (°) for monoclinic-**1**

Ba(1)—O(1)	2.803(6)	Mn(1)—O(4)	2.165(6)
Ba(1)—O(1′)	2.717(6)	Mn(1)—O(5)	2.158(5)
Ba(1)—O(2)	2.956(6)	Mn(1)—O(6)	2.833(6)
Ba(1)—O(3)	2.802(5)	P(1)—O(1)	1.520(6)
Ba(1)—O(4)	2.942(5)	P(1)—O(2)	1.513(6)
Ba(1)—O(5)	2.776(6)	P(1)—O(6)	1.503(7)
Ba(1)—O(6)	2.685(6)	P(1)—O(7)	1.590(6)
Ba(1)—O(6′)	2.672(6)	P(2)—O(3)	1.514(6)
Mn(1)—O(1)	2.249(5)	P(2)—O(4)	1.510(6)
Mn(1)—O(2)	2.059(6)	P(2)—O(5)	1.525(6)
Mn(1)—O(3)	2.124(5)	P(2)—O(7)	1.622(6)

O(1)—Mn(1)—O(2)	90.7(2)	O(2)—Mn(1)—O(6)	81.7(2)
O(1)—Mn(1)—O(3)	163.1(2)	O(3)—Mn(1)—O(4)	119.3(2)
O(1)—Mn(1)—O(4)	77.4(2)	O(3)—Mn(1)—O(5)	90.7(2)
O(1)—Mn(1)—O(5)	85.5(2)	O(3)—Mn(1)—O(6)	106.2(2)
O(1)—Mn(1)—O(6)	56.9(2)	O(4)—Mn(1)—O(5)	92.9(2)
O(2)—Mn(1)—O(3)	88.2(2)	O(4)—Mn(1)—O(6)	134.3(2)
O(2)—Mn(1)—O(4)	102.4(2)	O(5)—Mn(1)—O(6)	82.3(2)
O(2)—Mn(1)—O(5)	163.0(2)		

Estimated standard deviations in the least significant figure are given in parentheses.

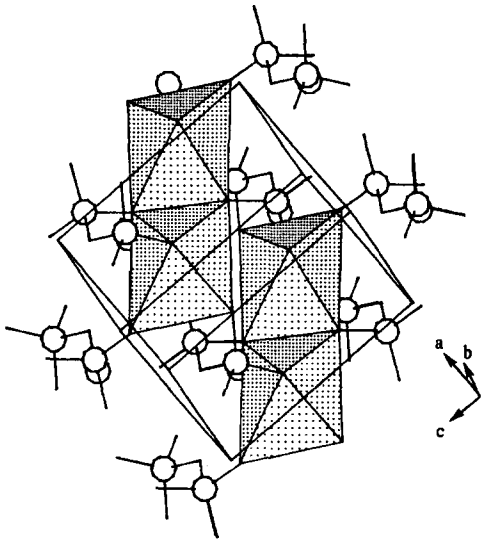

Fig. 2. A projection of the solid-state structure of $BaMnP_2O_7$, triclinic-**2**. The polyhedra show the coordination about the Mn^{2+} ions. Bonds between the phosphorus (large circles) and oxygen atoms are shown but the oxygen atoms are not drawn. The contacts to the barium atoms (small circles) are not drawn.

Description of the structure of $CaMnP_2O_7$ (**3**)

A projection of the solid-state structure of **3** is shown in Fig. 3. A list of selected bond distances and angles is given in Table 4. Each manganese ion in **3** is also surrounded by an octahedral arrangement of six oxygen atoms; however, the contacts

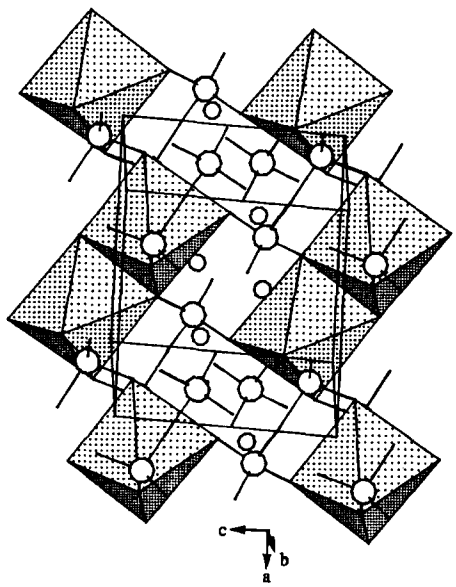

Fig. 3. A projection of the solid-state structure of $CaMnP_2O_7$ (**3**). The polyhedra show the coordination about the Mn^{2+} ions. Bonds between the phosphorus (large circles) and oxygen atoms are shown but the oxygen atoms are not drawn. The contacts to the calcium atoms (small circles) are not drawn.

Table 3. Selected interatomic distances (Å) and angles (°) for triclinic-**2**

Ba(1)—O(1)	2.917(5)	Mn(1)—O(5)	2.213(7)
Ba(1)—O(1′)	2.763(4)	Mn(1)—O(5′)	2.257(5)
Ba(1)—O(2)	2.924(5)	Mn(1)—O(6)	2.955(8)
Ba(1)—O(3)	2.989(5)	Mn(1)—O(7)	2.095(5)
Ba(1)—O(3′)	2.879(5)	P(1)—O(4)	1.611(6)
Ba(1)—O(3″)	2.698(5)	P(1)—O(5)	1.535(7)
Ba(1)—O(5)	2.976(5)	P(1)—O(6)	1.485(7)
Ba(1)—O(6)	2.749(6)	P(1)—O(7)	1.512(5)
Ba(1)—O(7)	2.774(5)	P(2)—O(1)	1.520(5)
Mn(1)—Mn(1′)	3.413(3)	P(2)—O(2)	1.519(5)
Mn(1)—O(1)	2.122(5)	P(2)—O(3)	1.504(6)
Mn(1)—O(2)	2.108(5)	P(2)—O(4)	1.608(5)

O(1)—Mn(1)—O(2)	89.0(2)	O(2)—Mn(1)—O(7)	67.4(2)
O(1)—Mn(1)—O(4)	122.8(2)	O(4)—Mn(1)—O(5)	129.0(2)
O(1)—Mn(1)—O(5)	87.7(2)	O(4)—Mn(1)—O(6)	61.1(2)
O(1)—Mn(1)—O(6)	71.0(2)	O(4)—Mn(1)—O(7)	84.2(1)
O(1)—Mn(1)—O(7)	119.4(1)	O(5)—Mn(1)—O(6)	158.5(2)
O(2)—Mn(1)—O(4)	124.0(2)	O(5)—Mn(1)—O(7)	107.7(2)
O(2)—Mn(1)—O(5)	103.4(2)	O(6)—Mn(1)—O(7)	139.6(2)
O(2)—Mn(1)—O(6)	74.3(2)	O(7)—Mn(1)—O(7′)	76.6(2)

Estimated standard deviations in the least significant figure are given in parentheses.

Table 4. Selected interatomic distances (Å) and angles (°) for **3**

Mn(1)—Mn(1′)	3.465(1)	Ca(1)—O(6)	2.441(3)
Mn(1)—O(1)	2.201(3)	Ca(1)—O(6′)	3.053(3)
Mn(1)—O(2)	2.205(3)	Ca(1)—O(7)	2.723(3)
Mn(1)—O(3)	2.256(3)	P(1)—O(1)	1.501(3)
Mn(1)—O(6)	2.242(2)	P(1)—O(2)	1.521(2)
Mn(1)—O(7)	2.289(3)	P(1)—O(3)	1.512(2)
Mn(1)—O(7′)	2.260(3)	P(1)—O(4)	1.622(3)
Ca(1)—O(1)	2.508(2)	P(2)—O(4)	1.582(2)
Ca(1)—O(2)	2.347(3)	P(2)—O(5)	1.500(3)
Ca(1)—O(3)	2.583(3)	P(2)—O(6)	1.518(3)
Ca(1)—O(5)	2.327(3)	P(2)—O(7)	1.536(2)
Ca(1)—O(5′)	2.390(2)		

O(1)—Mn(1)—O(2)	89.3(1)	O(3)—Mn(1)—O(4)	77.23(8)
O(1)—Mn(1)—O(3)	162.8(1)	O(3)—Mn(1)—O(5)	113.96(8)
O(1)—Mn(1)—O(4)	119.92(9)	O(3)—Mn(1)—O(6)	93.1(1)
O(1)—Mn(1)—O(5)	114.49(8)	O(3)—Mn(1)—O(7)	76.8(1)
O(1)—Mn(1)—O(6)	76.1(1)	O(4)—Mn(1)—O(5)	119.47(6)
O(1)—Mn(1)—O(7)	98.6(1)	O(4)—Mn(1)—O(6)	132.71(7)
O(2)—Mn(1)—O(3)	103.8(1)	O(4)—Mn(1)—O(7)	123.67(8)
O(2)—Mn(1)—O(4)	61.59(9)	O(5)—Mn(1)—O(6)	70.97(7)
O(2)—Mn(1)—O(5)	137.21(9)	O(5)—Mn(1)—O(7)	77.57(8)
O(2)—Mn(1)—O(6)	88.2(1)	O(6)—Mn(1)—O(7)	97.8(1)
O(2)—Mn(1)—O(7)	93.23(9)	O(7)—Mn(1)—O(7′)	80.8(1)

Estimated standard deviations in the least significant figure are given in parentheses.

are much more uniform than those in triclinic-**2**, and all six distances lie within the range 2.201(3)–2.289(3) Å. Compound **3** is isomorphous and isostructural to the previously reported compound $CaCo(P_2O_7)$.[2c] As in **2**, the manganese ions are also arranged in pairs through the formation of Mn_2O_{10} dinuclear groups in which two octahedra share a common edge. They differ, however, in the coordination of the P_2O_7 groups. In **2**, two of the P_2O_7 groups are arranged in the Mn_2O_{10} groups in bridge-apical sites, whereas in **3** these P_2O_7 groups occupy bridge-equatorial sites in the Mn_2O_{10} units.[2c] As in **2**, there is a short Mn···Mn contact, 3.465(1) Å, within each Mn_2O_{10} group. The Mn_2O_{10} groups are also joined via O—P—O links to six nearest-neighbour Mn_2O_{10} groups. The average P—O bond distance is 1.537 Å. The P—O bonds involving the bridging P—O—P atom, O(4), are again the longest, P(1)—O(4) = 1.622(3) and P(2)—O(4) = 1.582(2) Å. One PO_4 tetrahedron per diphosphate group has a free oxygen which participates in the coordination of the Ca^{2+} ion. The coordination of the calcium ion consists of seven closely positioned oxygen atoms with an average distance of 2.474 Å, and one at a substantially longer value, 3.053(3) Å.

Magnetic measurements

Because of the persistent contamination of the monoclinic form of $BaMn(P_2O_7)$ (**1**) by the triclinic form, **2**, no magnetic measurements of **1** were attempted.

The plots $1/\chi$ vs. T for **2** and **3** are shown in Figs 4 and 5, respectively. Both compounds are paramagnetic down to 5 K. The effective magnetic moments, μ_{eff} (corrected for TIP, see below), that were calculated for **2** and **3** are 5.7 and

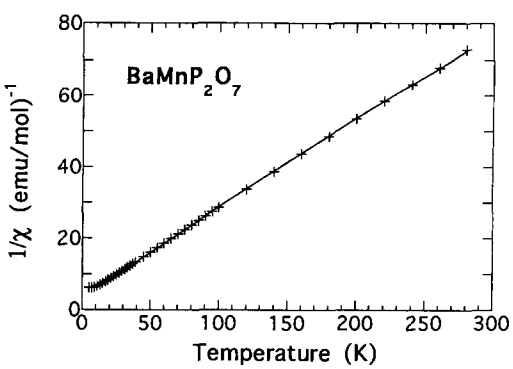

Fig. 4. A plot of the magnetic susceptibility $1/\chi$ versus T for triclinic-**2** in the range 5–300 K.

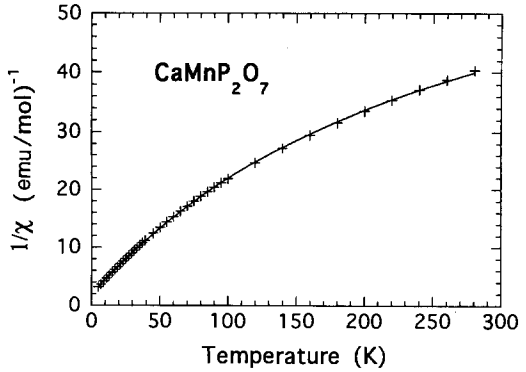

Fig. 5. A plot of the magnetic susceptibility $1/\chi$ versus T for **3** in the range 5–300 K.

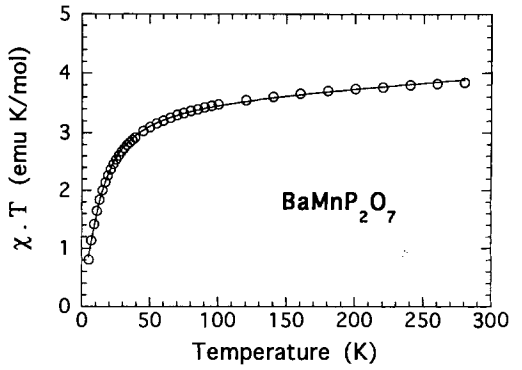

Fig. 6. A plot of the product χT vs. T for **2** in the range 5–300 K.

5.8 = B.M./Mn, respectively. Both of these values are consistent with Mn^{2+} in an octahedral environment having five unpaired electrons.

Since the structures of both of these compounds contain edge-shared (Mn_2O_{10}) bioctahedra, the presence of magnetic coupling between the manganese ions was anticipated. As a basis for the interpretation of the magnetic data, the simple isotropic Heisenberg Hamiltonian for two spin 5/2 paramagnetic centres was used (i.e. high-spin Mn^{II}) having no orbital angular momentum associated with ground states, irrespective of the symmetry of the environment):

$$H = -2J S_1 \cdot S_2.$$

J is the exchange coupling constant (negative for an antiferromagnetic AF interaction, positive for a ferromagnetic F interaction). The theoretical expression for the susceptibility χ is obtained by using the Van Vleck equation, and the experimental data were fit using the following expression for χ:[7]

$$\chi = \frac{Ng^2\mu_B^2(e^{2x}+5e^{6x}+14e^{12x}+30e^{20x}+55e^{30x})}{k(T-\theta)(1+3e^{2x}+5e^{6x}+7e^{12x}+9e^{20x}+11e^{30x})} + TIP,$$

where $x = -J/kT$.

A Weiss constant θ was included in the theoretical expression to allow for interdimer interactions, thus θ is not a true paramagnetic Curie temperature. A TIP term was added to take into account systematic errors or the presence of a small amount of diamagnetic impurities. Using $g = 2.0$, as expected for high-spin Mn^{2+}, the following values were obtained for the best fit, as represented in Figs 4 and 5.

For $BaMnP_2O_7$: $J/k = -1.47(3)$ K; $\theta = 1.3(1)$ K; $TIP = 0.0015(1)$ emu mol^{-1}.

For $CaMnP_2O_7$: $J/k = -1.04(3)$ K; $\theta = 2.3(1)$ K; $TIP = 0.0134(1)$ emu mol^{-1}.

If $\theta = 2z'J'/k$, where J' is the interdimer coupling constant and z' the number of nearest-neighbour binuclear units ($z' = 6$, for both compounds), then $|J'/J| = 0.18$ and 0.074 and for $BaMnP_2O_7$ and $CaMnP_2O_7$, respectively. As can be seen, the experimental results are accurately reproduced by assuming $S = 5/2$ antiferromagnetic dimanganese systems with $|J/k| = 1-1.5$ K. This is in agreement with structural findings, as well as the observed decreases of the χT products with decreasing temperature, see Figs 6 and 7. Note that the relatively small values of J have produced appreciable deviations from Curie law behaviour, as observed. This sensitivity of the susceptibility of the $S = 5/2$ binuclear system to small values of J arises because of the relatively large spread in energy of the spin states (the total spread is $|30J|$). The intradimer interactions are, however, too small compared with the lowest temperatures that were used to detect the susceptibility maximum expected for such AF dimers. It is notable that in the absence of the antiferromagnetic interactions between the manganese ions, the susceptibility would obey a Curie law and

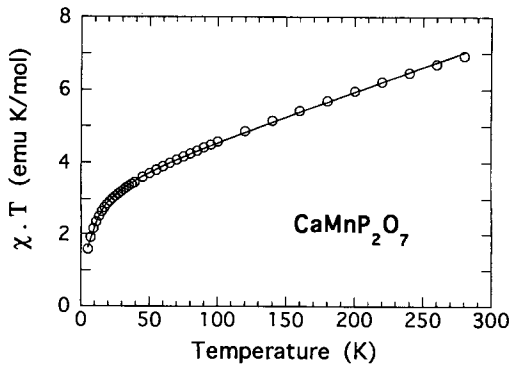

Fig. 7. A plot of the product χT vs. T for **3** in the range 5–300 K.

μ_{eff} would be equal to the spin-only value 5.92 B.M. both for triclinic-**2** and -**3**.

Supplementary materials available. Tables of positional parameters, anisotropic thermal parameters and structure factor amplitudes (25 pages) for the structural analyses are available from the authors (R.D.A.).

REFERENCES

1. (a) K. H. Lii, Y. P. Wang, Y. B. Chen and S. L. Wang, *J. Solid State Chem.* 1990, **86**, 143; (b) E. A. Genkina, B. A. Maksimov, V. A. Timofeeva, A. B. Bykov and O. K. Mel'nikov, *Sov. Phys. Dokl.* 1985, **30**, 817; (c) S. L. Wang, P. C. Wang and Y. P. Nieh, *J. Appl. Cryst.* 1990, **23**, 520; (d) Y. P. Wang, K. H. Lii and S. L. Wang, *Acta Cryst.* 1989, **C45**, 673; (e) A. Leclaire, M. M. Borel, A. Grandin and B. Raveau, *J. Solid State Chem.* 1988, **76**, 131; (f) M. Gabelica-Robert, M. Goreaud, Ph. Labbe and B. Raveau, *J. Solid State Chem.* 1982, **45**, 389; (g) J. P. Gamondes, F. D'Yvoire and A. Boulle, *C. R. Acad. Sci. Paris Ser. C* 1969, **269**, 1532; (h) Y. P. Wang and K. H. Lii, *Acta Cryst.* 1989, **45**, 1210; (i) L. Benhamada, A. Grandin, M. M. Borel, A. Leclaire and B. Raveau, *Acta Cryst.* 1991, **C47**, 424; (j) K. H. Lii and R. C. Haushalter, *Acta Cryst.* 1987, **C43**, 2036; (k) D. Riou, A. Leclaire, A. Grandin and B. Raveau, *Acta Cryst.* 1989, **C45**, 989; (l) J. J. Chen, C. C. Wang and K. H. Lii, *Acta Cryst.* 1989, **C45**, 673; (m) A. Leclaire, M. M. Borel, A. Grandin and B. Raveau, *J. Solid State Chem.* 1989, **78**, 220; (n) D. Riou, Ph. Labbe and M. Goreaud, *Eur. J. Solid State Inorg. Chem.* 1988, **25**, 215; (o) E. Dvoncova and K. H. Lii, *J. Solid State Chem.* 1993, **105**, 279.
2. (a) D. Riou and B. Raveau, *Acta Cryst.* 1991, **C47**, 1708; (b) D. Riou and M. Goreaud, *Acta Cryst.* 1990, **C46**, 1191; (c) D. Riou, P. Labbe and M. Goreaud, *C. R. Acad. Sci. Paris* 1988, **307**(II), 1751; (d) A. Moqine, A. Boukhari and E. M. Holt, *Acta Cryst.* 1991, **C47**, 2294; (e) D. Riou, P. Labbe and M. Goreaud, *C. R. Acad. Sci. Paris* 1988, **307**(II), 903; (f) D. Riou, H. Leligny, C. Pham, P. Labbe and B. Raveau, *Acta Cryst.* 1991, **B47**, 608; (g) M. V. Hoffman, *J. Electrochem. Soc.* 1963, **110**(12), 1223.
3. (a) T. Ericsson and A. G. Nord, *Acta Chem. Scand.* 1990, **44**, 990; (b) J. A. R. Stiles and C. V. Stager, *Can. J. Phys.* 1973, **51**, 87; (c) D. C. Fowlis and C. V. Stager, *Can. J. Phys.* 1969, **47**, 371; (d) M. F. Collins, G. S. Gill and C. V. Stager, *Can. J. Phys.* 1971, **49**, 979; (e) D. C. Fowlis and C. V. Stager, *Can. J. Phys.* 1972, **50**, 2681; (f) J. B. Forsyth, C. Wilkinson, S. Paster and B. Wanklyn, *J. Phys. Condens. Mat.* 1989, **169**, 20; (g) B. E. Robertson and C. Calvo, *Can. J. Chem.* 1968, **46**, 605; (h) B. E. Robertson and C. Calvo, *Acta Cryst.* 1967, **22**, 665; (i) T. Stefanidis and A. G. Nord, *Acta Cryst.* 1984, **C40**, 1995; (j) H. Effenberger, *Acta Cryst.* 1990, **C46**, 691.
4. (a) A. Handizi, A. Boukhari, E. M. Holt, J. Aride and S. Flandrois, *Mater. Res. Bull.* 1993, **28**, 1241; (b) K. Benkhouja, M. Zahir, A. Sadel, A. Handizi, A. Boukhari, E. M. Holt, J. Aride and M. Drillon, *Mater. Res. Bull.* 1995, **30**, 49; (c) A. Handizi, A. Boukhari, E. M. Holt, J. Aride, M. Belaiche and M. Drillon, *Eur. J. Solid State Inorg. Chem.* 1994, **31**, 123; (d) A. ElMaadi, A. Boukhari, E. M. Holt and S. Flandrois, *J. Alloys Comp.* 1994, **205**, 243.
5. (a) *International Tables for X-ray Crystallography*, Vol. IV, Table 2.2B, pp. 99–101. Kynoch Press, Birmingham, England, (1975); (b) *ibid.*, Table 2.3.1, pp. 149–150.
6. C. Calvo, *Inorg. Chem.* 1968, **7**, 1345.
7. F. E. Mabbs and D. J. Machin, *Magnetism and Transition Metal Complexes*, Ch. 7. Chapman & Hall, London (1973).